

## **The development of an ultrasonic measurement for the prediction of paper strength properties – Part I.**

**R J Allan.**

Technical Director, XQ innovations P/L  
Mt Waverley,  
Melbourne,  
Australia.

### **Abstract**

Non-destructive and continuous measurement of strength during the making of paper has been an aspirational objective for the paper industry over the last 30 years. The major issues that have made progress in this area slow and have frustrated general implementation include difficulty in suppressing unrelated noise during measurement and the inability to usefully match the raw property measured by ultrasonic testers (generally, extensional stiffness) and those standard properties typically used to reflect paper quality.

Variation of strength paper properties during the manufacturing process, unrelated to mass or thickness variation, has been estimated to be between 10 to 30% and is dependent upon the design of the paper machine, furnish and the chosen machine operating conditions. A method suitable for on-line estimation of desirable strength properties, such as ring crush and tensile strength, has been developed using ultrasonic measurement. The proposed method overcomes the problems that made previous measurement methods impractical.

This paper describes the measurement concepts that allow the use of ultrasonic measurement to progress to a form that is suitable for on-line measurement on the paper machine and presents correlations that relate common quality properties such as ring crush and tensile to the raw sonic test measurement.

Further, the implementation of a fast, non-destructive and accurate estimation of paper strength property allows enough data to be collected, at an appropriate

scale, to begin the process of understanding the cause of run-of-mill paper strength variation.

### **Introduction**

In 1979 a seminal paper by Mann et al <sup>(1)</sup> was published describing the use of ultrasonic wave propagation to estimate the elastic constants associated with paper. The paper was the forerunner of a larger body of work aimed at introducing in-plane measurement of paper elastic constants to the paper machine <sup>(2-6)</sup>. Subsequently, out-of-plane measurement systems were developed by Brodeur and Hall <sup>(2)</sup>, and others. For over three decades attempts to provide reliable, continuous on-line paper stiffness measurements have been on-going, but, largely unsuccessful. Several paper industry, industry technical institutions and government bodies have invested heavily in the attempt to develop a practical commercial on-line system <sup>(3,4,5)</sup>, the most recent being a laser based interferometry method purported to satisfactorily measure bending stiffness on the paper machine in real time <sup>(11)</sup>.

In parallel with the practical implementation efforts a growing body of theoretical and laboratory work relating commonly measured paper properties to various amalgams of paper elastic constants had been amassed. Some of the relationships – such as for short span compression, bending stiffness and extensional stiffness give impressive correlations, albeit for a limited range of process and furnish parameters <sup>(6-8)</sup>.

These efforts were not just confined to contact ultrasonic systems but included non-contact sonic measurements, mechanical systems, rubber wheels and laser interferometry <sup>(9-12)</sup>.

The development of non-destructive methods for elastic constant determination of paper gave new insights into the effect of operational settings such as pressing, refining, drying restraint, draws and calendering <sup>(13-16)</sup>. These findings were facilitated by the increased data rates that non-destructive sonic testing provides.

It soon became clear that the property variability from moment to moment on a commercial paper machine was extremely high. More alarming was the realisation that this property variability was not related to mass or thickness variations on the paper machine but must be attributed to material or structural variation in the formed sheet itself. CD variation in strength is generally attributed to CD drying variation, fibre orientation and the variation of drying restraint and Poisson tensioning processes in free draws down the paper machine<sup>(17)</sup>. The strength variation across commercial paper machines can be as much as 30%. This variation level and shape is a signature for a given machine and is a relatively stationary characteristic of a particular machine design.

Of equal interest is what happens to property variability in the machine direction of the paper machine. Variation in this direction appears to range between around 10% and 20% for properties like ring crush<sup>(17)</sup>. Causes of grammage-unrelated md strength variation have been vague and are an important part of this work.

The need to understand the sources and mechanistic causes of machine direction paper strength variation is important because, unlike the cross direction variation that is largely fixed by machine design and requires expensive re-builds to improve, a significant proportion of the machine direction variation can be attributed to longer term changes that can (theoretically) be removed or lessened by standard process control methods. What is needed is a suitable, continuous, on-line measurement sensor to provide the error signal to a suitable process controller.

A review of relevant literature shows there are a number of issues that must be overcome if a useful on-line measurement is to be developed<sup>(18)</sup>:

- Signal to noise ratios must be kept high.
- Stray paths must be eliminated (air, mechanical and radio interference).

- Time delayed reflections from free edges of the paper must be dealt with
- Wave mode conversions occurring at the edge of the paper sheet must be dealt with.
- The unit must be robust and capable of surviving the rigours of the paper machine.
- It must deliver a result that relates to meaningful properties or performance.
- Ringing of the receive transducer must be accounted for or eliminated (especially if the measurement is undertaken around the sensor resonance frequency).

XQi's response to the problems that have thwarted previous attempts at on-line measurement are to:

- Utilise continuous wave measurement technology.
- Apply a time delay spectrometry (TDS) approach to analysis of the signal waves.
- Ensure the measurement carriage is rolling and frictionless and that the measurement itself is not dependent on the structural contacting element.
- Successfully develop property algorithms that predict properties such as ring crush to a useful accuracy

### *Ultrasonic paper measurement*

Traditionally, ultrasonic measurement of paper has been undertaken by estimating the propagation delay between an ultrasonic wave launched at a transmitter and the same wave captured by a receiver a known distance away. The velocity of the sonic wave can then be calculated as:

$$c = d / t \quad [1]$$

Where

$c$  is the velocity in m/sec  
 $d$  is the distance travelled between the transmitter and receiver (meters) and  
 $t$  is the time in seconds.

The modulus is calculated as:

$$E_s = \rho c^2 (1 - \nu_{xy} \nu_{yx}) \quad [2]$$

To a good approximation the term in brackets will be around 0.9 – 1.0 for papers made at commercial md-to-cd ratios <sup>(20)</sup>, and so an often used representation to the modulus is taken as the “sonic” modulus,  $E_s$ :

$$E_s \approx \rho c^2 \quad [3]$$

Where  $\rho$  is the apparent density of the paper sheet in  $\text{kg/m}^3$ ,  $\nu_{xy}$  and  $\nu_{yx}$  are the in-plane Poisson ratios and  $c$  is the low frequency symmetric wave velocity mode. It becomes clear that for fixed distance sensors, the velocity determination requires a measurement of the propagation delay of the transmitted wave. In its simplest realisation a pulse is propagated through the material and the propagation delay between two fixed points is measured.

Figure 1 shows the paths that might be set up in a typical static (constant frequency) ultrasonic measurement. Figure 2 shows the summing of a simple, two path, constant frequency system showing the individual wave components for each path and their relative phase delay. As shown in figure 2 the signal that is received at the receiver is very different from the direct (desired) path signal, and it is clear that to

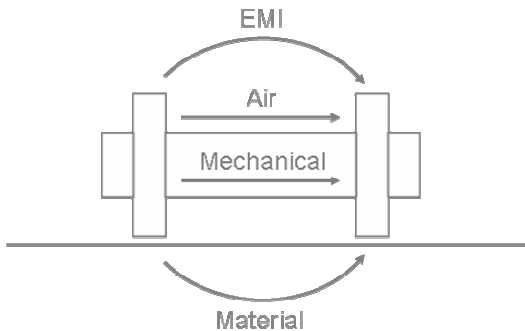


**Figure 1. Schematic representation of different competing paths in the sensor-paper system.**

properly measure the phase delay of a continuous frequency signal, the spurious or non-measurement related paths must have their magnitude limited to a very low level.

$$f_s = f_{emi} + f_{mech} + f_{air} \quad [4]$$

The sum of sine waves is given as:

$$\begin{aligned} & \sin(\omega_1 t) + \sin(\omega_2 t) \\ &= 2 \sin\left(\frac{\omega_1 + \omega_2}{2} t\right) \cos\left(\frac{\omega_1 - \omega_2}{2} t\right) \end{aligned} \quad [5]$$

It is apparent from the identity above that the result of *adding* two sine waves of different frequencies is to produce a modulated signal with carrier frequency  $(\omega_1 + \omega_2)$  and modulation frequency  $(\omega_1 - \omega_2)$ . If  $\omega_1 = \omega_2$  then the identity collapses to a sine wave with the original frequency, the sum of the magnitudes and, if the component phases are non-zero, with a phase equal to one half the sum of the component phases.

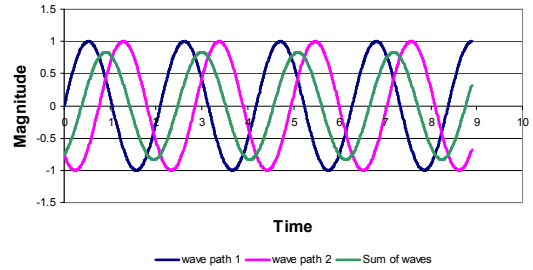


**Figure 2. Two waveforms, one with a propagation delay compared to the other. The green waveform is the sum of the two input waveforms.**

A trigonometric identity shown in equation [6] gives the relationship between superposed waveforms of different but constant phase and the same frequency:

$$A \sin(\omega t) + B \sin(\omega t + \phi) = C \sin(\omega t + \beta) \quad [6]$$

Where,

$$C = \sqrt{A^2 + B^2 + 2AB \cos \phi}, \quad [7]$$

and

$$\beta = \arctan\left(\frac{B \sin \phi}{A + B \cos \phi}\right) \quad [8]$$

From the above simple system of two paths we can see that the final phase is dependent upon both the magnitude of the two signals and their respective phase.

If we assume the overall interference effect can be given by:

$$f_s = B \sin(\omega t + \phi) \quad [9]$$

Where  $\phi$  is the resultant phase of the interfering effects and  $B$  is the magnitude of the interfering waveform.

From equation [2], [3] and [4], the resulting waveform phase can be calculated.

By setting the relative values for  $A$  and  $B$ , and for  $\phi$ , a sensitivity analysis for this simple system can be constructed that estimates the error brought about by the superposition of paths other than the material measurement path.

### Sensitivity analysis.

Figure 3 shows the simplest case of one transmitted planar wave and the minimum number of possible components received at the receiver at time  $t$ . To aid

visualisation of the problem it is assumed that the transmit signal is a constant frequency sinusoid of constant amplitude,  $A \sin(\omega t + \phi)$ , where the phase  $\phi$  is taken to be zero.

For this example constant material wave component magnitude of 500 mV and zero phase was used while the interfering waveform was varied from 0 to 500 mV in 50 mV steps for magnitude and 0 to 180° in 10° steps for the interfering wave phase. The error is calculated as percentage of the period of the waveform (that is the phase or delay error).

The figure shows that to keep error from interfering paths to less than 1% requires the interfering paths to be less than 2% of the magnitude of the desired wave path signal. Suppression of interfering wave paths to this level is very difficult indeed.

In part, this is one of the reasons why pulsed measurement has been persevered with for so long. Measuring the arrival of a pulse or suitable “burst”, in effect separates interfering paths in the time domain. The direct path will generally arrive first (ignoring any electromagnetic interference) followed by propagation paths with greater delay times. Of course, the disadvantage of using a pulsed signal or burst wave is that in the frequency

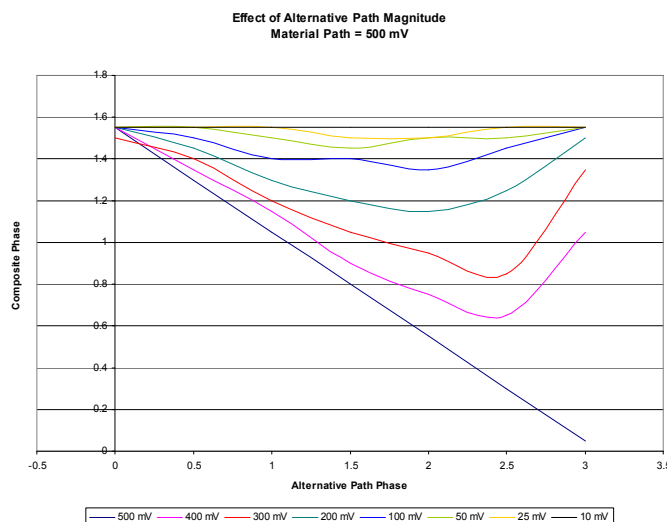


**Figure 3. The graph shows the effect of increasing magnitude of the interfering waveform (alternate paths) as the phase of the alternate wave changes.**

domain the signal appears as a number of frequency components occurring over a wide frequency range. This has been shown to make the measurement sensitive to dispersion effects and distortion of the waveform due to the frequency components of the transmitted wave shape being delayed at different rates<sup>(22,24)</sup>. When these dispersive components are re-combined at the transmitter they form a distorted representation of the original transmission. In some cases this distortion makes the determination of the exact propagation delay time of a pulse difficult to extract. This effect will be more noticeable when measuring heavier packaging grades.

### ***Time delay spectrometry***

Time delay spectrometry is an analysis technique that has been applied to acoustic characterisation of aural spaces<sup>(21)</sup>. Early in the development cycle of measurements for paper properties the TDS method was considered a potentially robust measurement method as it utilises a continuous wave excitation signal. However, TDS was soon abandoned as the issue of reflections interfering with the continuous wave phase was found to be an insurmountable problem and TDS was unable to provide adequate time resolution<sup>(18)</sup>.

The TDS technique relies on the separation of delayed signals and their subsequent transformation between the time and frequency domains by multiplying the original and delayed waveforms. Careful use of a swept frequency wave as the transmitted excitation signal has the affect of limiting the measurement requirement to one of measuring a frequency difference between the transmit wave and receive wave. Proper setting of the sweep time and frequency change allows individual delay paths that might add together at the receiver to be separated in the frequency domain.

The linear frequency sweep can be represented as:

$$F(t) = \sin(St^2 + \omega_0 t + \phi) \quad 0 < t < T \quad [10]$$

where

$S$  is the frequency sweep rate in radians/s<sup>2</sup>,  
 $\omega_0$  is the starting frequency of the sweep (radians/s)

$\phi$  is the initial phase (radians) and

$T$  is the duration of the sweep in seconds

$$\begin{aligned} & \sin(\omega_1 t) \cdot \sin(\omega_2 t) \\ &= \frac{1}{2} [\cos((\omega_1 - \omega_2)t) - \cos((\omega_1 + \omega_2)t)] \end{aligned} \quad [11]$$

Low pass filtering the product of the multiplication gives the lower frequency component:

$$\sin(\omega_1 t) \cdot \sin(\omega_2 t) = \frac{1}{2} \cos((\omega_1 - \omega_2)t) \quad [12]$$

The frequency difference component represents the difference in frequency between the two multiplied signals. In the context of the linear swept wave approach, knowing the rate for the frequency sweep,  $S$ , allows the frequency difference to be converted into a propagation delay.

The instantaneous frequency measured at any point in time is not frequency in the Fourier sense<sup>(23)</sup>. And to some extent we take a liberty to define a frequency-like parameter. Strictly speaking we should use the term “the derivative of the time domain phase”. However, for convenience and under certain circumstances instantaneous frequency has some resemblance to frequency in the Fourier sense and we will persevere with this definition - keeping in mind that  $f_i$  is really a time domain description of the signal.

In the simplest terms, the equations representing the TDS excitation waveforms and analysis may be considered to be a prescription that converts frequency into time of on-going human experience and hence delays into frequency shifts.

$$f_1(t) = \frac{1}{2} \sin(St^2 + \omega_1 t) \quad [13]$$

$$f_2(t) = \frac{1}{2} \sin(St^2 + (\omega_1 - St_d)t) \quad [14]$$

Where  $f_1$  is the transmitted frequency sweep,  $f_2$  is the received (and delayed) signal and  $t_d$  is the component path propagation delay.

Multiplying equations [9] and [10] together to take advantage of the identity in equation [7] and removing the high frequency term gives:

$$f_1(t) \times f_2(t) = \frac{1}{2} \sin[(\omega_1 - \omega_2 + St_d)t] \quad [15]$$

$$f_1(t) \times f_2(t) = \frac{1}{2} \sin[(\Delta\omega + St_d)t] \quad [16]$$

As the sweeps are correlated (notionally delayed versions of each other),  $\Delta\omega$  would normally be set to zero.

In more general terms and including all the possible paths we can write for the resultant waveform:

$$F(t) = \sum_{n=0}^N \frac{1}{2} \sin(\Delta\omega + St_{d_n})t \quad [17]$$

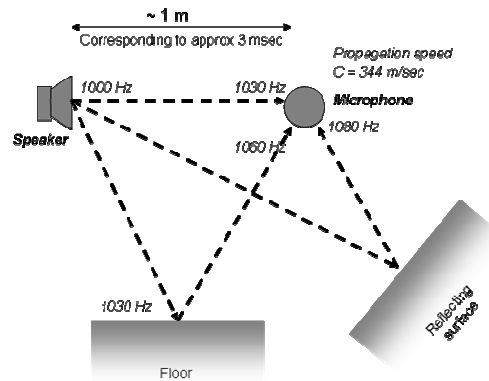
Where  $\Delta\omega$  represents any frequency differences in the reference and transmit sweep waves and  $St_d$  is the frequency representation associated with the propagation delays.

Equation [17] is the essence of the presented TDS method and as a linear sweep is used the conversion factor becomes equal to the sweep rate  $S$ . The conversion can be very simply illustrated with an example<sup>(23)</sup> based on characterisation of the sound response of a speaker in a room.

### TDS Example

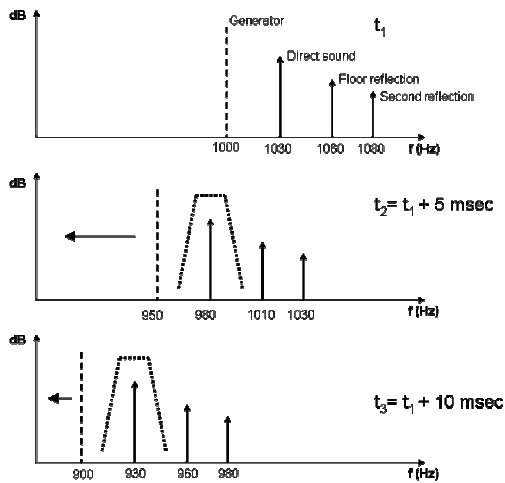
Figure 4 shows a typical application employing TDS, where the free-field response of a loudspeaker has to be measured in an ordinary room. When employing a linear sweep, the various delays will be converted into frequency shifts proportional to the delay and sweep rate,  $S$ . The figure shows the frequencies present at the microphone at the moment in time when the generator is at 1000 Hz.

Figure 5 shows the spectrum at the microphone corresponding to three distinct times during the sweep.  $t_1$  corresponds to the instantaneous picture in Figure 4. During the sweep the whole picture will be shifted towards the lower frequencies but the relative position of the components remains unchanged. The levels of the individual components will change in accordance with the frequency responses. In this example the tracking filter is tuned to measure the direct sound.



**Figure 4. Reflections giving delayed paths.**

In a similar way to the described examples, propagation delays for the sonic measurement in paper can also be presented. For this test a 120 gsm semi-chem medium was used. The delays for each of the measured components were determined by filtering at various frequencies to only allow frequencies representing chosen delays in the system. The result of such a test made in the machine direction (with arbitrary frequency scaling) is depicted in Figure 7.



**Figure 5. Instantaneous frequencies at time  $t$  representing various delay paths**

### Calibration

The TDS method is well suited to separating separate paths with different delays. The original work by Baum et al<sup>(3)</sup> used a method to estimate the latency attributable to electronics that relied on multiple measurements. Delay measurements were made at various transducer distances and a plot was generated that allowed the delay at zero distance to be inferred. This delay represented the measurement delay due to electronics filtering and signal conditioning.

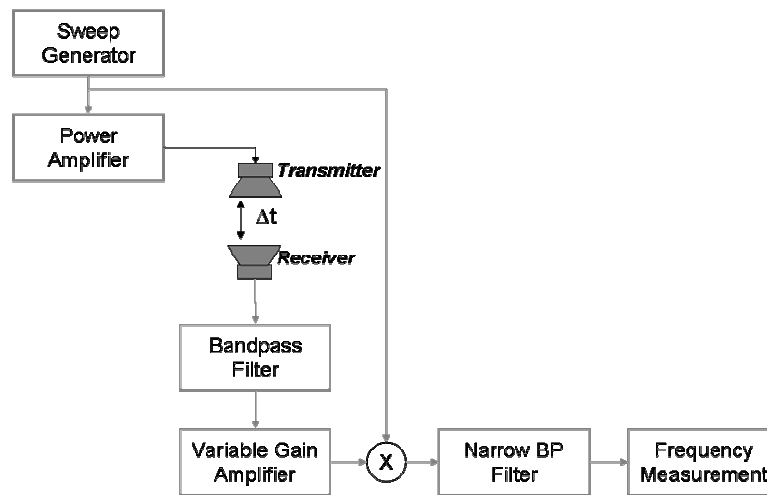


**Figure 6. Block diagram of TDS measurement system for ultrasonic paper measurement**

Table I shows a range of potential path parameters related to a specific instant in time. The table assumes a sweep rate,  $S$ , of 1MHz per second and a range of propagation delay times.

In the configuration used in this development, the distance between the transducers have been fixed so the method presented by Baum and Bornhoeft cannot be used.

**Table I. Typical propagation path parameters (assume  $S = 1\text{MHz/sec}$ )**

Path	Distance (mm)	Velocity (m/sec)	Delay ( $\mu\text{s}$ )	Relative Magnitude	$\Delta f$ (Hz)
Paper (CD)	65	2200	29.55	1.0	29.55
Paper (Shear)	100	1600	62.5	1.0	62.5
Air	65	330	197.0	0.1	197.0
Mechanical	100	3500	28.6	0.05	28.60
Material reflections	130	2200	59.09	0.2	59.09
EM interference	65	$3 \times 10^9$	0.00	0.05	0.00
Mode conversion	130	1100	118.2	0.05	118.2

Due to the ability of the TDS method to separate delay paths in time, separating the delay due to the residual air path becomes tractable. Whereas in other measurement schemas the air path becomes an interference that is difficult to remove, in the TDS implementation it becomes a potential method for calibration.

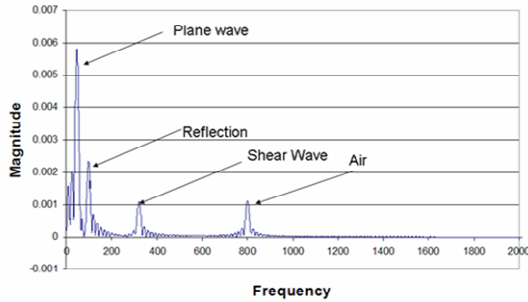


**Figure 7 shows characteristic results for a packaging paper measured in the machine direction ( $S = 2$  MHz/sec).**

The velocity of air can be calculated as:

$$c_{air} = 331.3 \sqrt{1 + \frac{v}{273.15}} \quad [9]$$

Where  $c_{air}$  is the velocity of sound in air (m/sec), and  $v$  is the temperature in degrees Celsius. The relationship in equation [9] changes slightly with humidity in the air (between 0.1%-0.6%) with the velocity slightly higher in humid air. The relationship hardly changes at all with changing pressure.

### Validation

Two validation methods are presented in this paper:

1. Polar stiffness plot
2. Calculation of the elastic constants of paper.

### Polar Stiffness Plot

Figure 8 presents in-plane wave velocity measurements taken at various angles to the machine direction of semi-chem medium paper. The plot shows a slight orientation angle away from the machine direction and the typical “peanut” shape

stiffness plot reported by many previous workers.

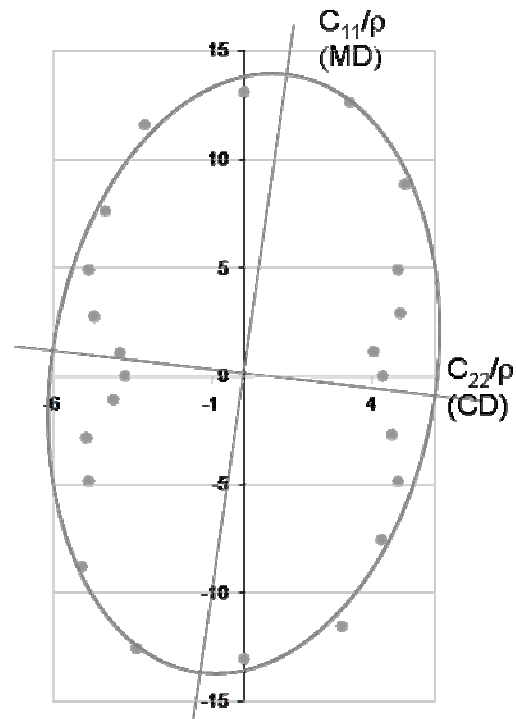


**Figure 8. Polar plot of sonic stiffness**

### Measurement of orthotropic elastic constants

As a final measure of support for the developed measurement system, the orthotropic elastic constants can be estimated and compared to values for paper found in the literature.

For an orthotropic material such as paper, the full description of the elastic stress-strain response requires nine material constants. Figure 9 shows three deformation modes in uniaxial tension and three deformation modes in shear where the arrows represent the application of the stress. Poisson ratios, that describe the interaction or the “connectivity” of any two principal directions, make up the remaining three constants required to fully describe the elastic response of paper.

$C_{11}$ ,  $C_{22}$ ,  $C_{33}$  and  $C_{66}$  can be measured directly as propagation delays.  $C_{12}$  can be estimated by propagating a shear wave at 45 degrees to the in-plane principal axes of the paper and using relationships developed by Habeger et al<sup>(3)</sup>.  $C_{55}$  and  $C_{44}$  are related to the onset of a Rayleigh type

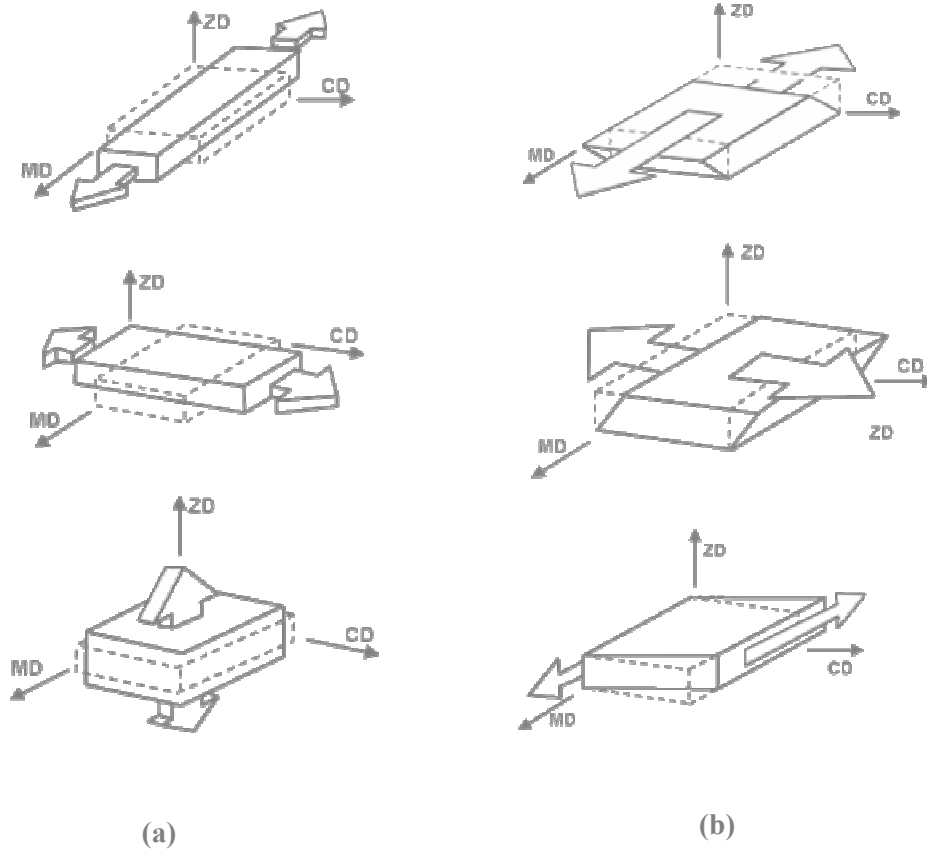


**Figure 9. Modes of deformation in (a) uni-axial tension and (b) shear after Baum (4).**

surface wave when measured in the md and cd directions respectively.  $C_{13}$  and  $C_{23}$  can be estimated from a measurement of the position of the vertical asymptotes of the generated dispersion curves in the machine and cross direction, where:

$$C_{13} = \sqrt{C_{33}(C_{11} - \rho V_{So_x}^2)} \quad [17]$$

$$C_{23} = \sqrt{C_{33}(C_{22} - \rho V_{So_y}^2)} \quad [18]$$

In this calculation  $C_{11}$ ,  $C_{22}$  are calculated using the velocity of the  $S_1$  symmetric mode wave in the  $x$  (md) and  $y$  (cd) direction respectively, while the  $So_x$  and  $So_y$  subscript represents velocities measured with the zeroth order symmetric mode.

From these constants it is then possible to estimate the three Poisson ratios  $\nu_{12}$ ,  $\nu_{13}$  and  $\nu_{23}$  using equations reported by Baum et al<sup>(3)</sup>, namely,

$$\begin{aligned} C_{12} &= \nu_{12} C_{11} \\ C_{23} &= \nu_{23} C_{22} \\ C_{13} &= \nu_{13} C_{11} \end{aligned} \quad [19]$$

$$\text{with} \quad C_{ij} = R_{ij} \nu_{ji} \quad [20]$$

where  $R_{ij}$  is the relevant stiffness ratio.

Table II compares the orthotropic elastic constants estimated in this work (a semi-chem 120 gsm medium and a recycled 150 gsm liner) with previously published values for a range of samples including liner<sup>(1)</sup>, medium<sup>(1)</sup>, milk carton board and chip board<sup>(1)</sup>.

**Table II. Ultrasonic estimates of the orthotropic elastic constants of paper.**

Samples	$C_{11}/\rho$	$C_{22}/\rho$	$C_{33}/\rho$	$C_{12}/\rho$	$C_{13}/\rho$	$C_{23}/\rho$	$C_{44}/\rho$	$C_{55}/\rho$	$C_{66}/\rho$	$\nu_{12}$	$\nu_{13}$	$\nu_{23}$
SC 120	11.6	4.84	0.13	-	-	-	.224	0.308	2.56			
RL 150	9.8	4.01	0.134	-	-	-	.210	0.285	2.34			
Carton stock	10.27	4.92	0.053	1.74	0.118	0.116	0.127	0.175	2.61	0.15	0.008	0.021
Chip board	10.24	3.474	0.076	-	0.322	0.249	0.156	0.220	2.31	-	-	-
Liner (90 lb)	8.12	3.32	0.032	1.19	0.113	0.082	0.104	0.129	2.89	0.117	0.011	0.021
Medium	13.18	4.928	-	-	-	-	-	-	3.20	-	-	-

Comparison of values in the table shows that the elastic constant estimates in this work are of the same order as that published previously and lends support to the currently described method.

### Dispersion Curve Generation

A TDS measurement system lends itself to characterising the stiffness response of paper in more general ways.

A proper description of the elastic response of orthotropic materials requires the specification of nine independent stiffness-coefficients (or elastic constants), relating the stress components to the strain components.

A plate of uniform thickness behaves as a waveguide for elastic waves; its dynamic response to a specified excitation can be expressed (in principle) as a superposition of its modes of free vibration. This characterisation can be made by the mode shape, describing the variation across the thickness of the elastic displacement  $\mathbf{u}$ , or of a stress component, and the dispersion curves which give the relation between the angular frequency  $\omega$  and the wave number  $k$ , or equivalently the relation between the phase velocity  $c$  and frequency  $\omega$ , for each separate mode.

The general features of the wave modes for an orthotropic plate are quite similar to those for an isotropic plate<sup>(23)</sup> with some complications and additional features due to anisotropy. In the case of orthotropic plates (paper is an example) greater complexity in the calculation is evident and can be attributed physically to the fact that the phase velocity for plane waves now depends on the direction of propagation. In a similar way to the

isotropic case, the equations of motion lead to two possible wave speeds for bulk plane waves, the associated deformations are no longer purely transverse or purely longitudinal, except when the direction of propagation coincides with a principal axis.

The dispersion relation is given by the following equation<sup>(9)</sup>

$$\frac{\tan(\beta h)}{\tan(\alpha h)} = \left[ \frac{H_m G_p}{H_p G_m} \right]^{\pm 1} \quad [10]$$

$$(\alpha/k)^2 = -B + \sqrt{(B^2 - 4D)/2} \quad [11]$$

$$(\beta/k)^2 = -B - \sqrt{(B^2 - 4D)/2} \quad [12]$$

Where the plus and minus sign in the exponent of equation [10] correspond to symmetric and anti-symmetric modes respectively.  $B$ ,  $D$ ,  $G_{p,m}$ , and  $H_{p,m}$ , are given by complicated expressions involving the orthotropic elastic constants which are not reproduced here.

It is enough to note that the right hand side of equation [12] depends only on the wave number  $k$  (or more precisely, the dimensionless quantity  $kh$ ) whereas  $\alpha$  and  $\beta$  depend in addition on the angular frequency  $\omega$ . From these equations the dispersion curves can be constructed by solving equation [12] for  $\omega$  as a function of  $k$ . The cut-off frequencies for higher order modes can be obtained by letting  $k$  approach 0, and the resulting motions interpreted as standing waves in the thickness direction ( $z$ ). Most importantly, when the dispersion curves are plotted as phase velocity  $c$  versus frequency  $\omega$ , as in Habeger et al<sup>(1)</sup>, the cut-off frequencies can

be readily identified by the fact that the curves exhibit a vertical asymptote as these frequencies are approached from above - a direct result of the much lower  $z_d$  stiffness (anisotropy) in paper.

The vertical asymptote frequencies in the  $md$  direction are given by:

$$\omega_n = \frac{2\pi n}{h} \sqrt{\frac{C_{11} C_{33} C_{55}}{\rho C_{13} (2C_{55} + C_{13}) + C_{11} C_{55}}} \quad [13]$$

With the upper and lower horizontal portions of the curve (velocities) approximately given respectively as:

$$c^2 = \frac{C_{11}}{\rho} \quad \text{or} \quad c^2 = \frac{C_{55}}{\rho} \quad [14]$$

Where  $C_{ij}$  are various stiffness values attributable to orthotropic plates,  $c$  is the phase velocity,  $\rho$  is the apparent density of the sheet and  $h$  is the apparent thickness of the sheet.

Note that the horizontal portions of the plot are independent of the thickness of the paper, whereas the vertical asymptotes are inversely related to the thickness and sensitive to the out-of-plane stiffness  $C_{33}$ . Further analysis would show that the vertical segments of the dispersion curve are insensitive to  $C_{55}$ , with smaller  $C_{13}$  values giving sharper drops in the curve response.

Assuming  $C_{13}$  is small and  $C_{13}^2 \ll 1$ , equation [13] can be simplified to give an approximate expression for the frequency position of the vertical asymptotes:

$$\omega_n = \frac{2\pi n}{h} \sqrt{\frac{C_{11} C_{33}}{\rho (2C_{13} + C_{11})}} \quad [15]$$

A further approximation – ignoring  $C_{13}$  altogether - will result in:

$$\omega_n = \frac{2\pi n}{h} \sqrt{\frac{C_{33}}{\rho}} \quad [16]$$

Thus the positioning of the vertical dispersion curve segments is mostly controlled by the out-of-plane stiffness  $C_{33}$  (which in paper is relatively low) and the paper thickness,  $h$ . Increasing paper thickness has the effect of lowering the frequency of the asymptotes and potentially moving any measurement into a dispersive region on the velocity-frequency mapping.

Armed with the above response equations for an orthotropic plate, it is possible to broadly map the dispersion curve for particular tested papers.

Figure 10 represents a schematic showing the theoretical asymptotic characteristics of the 120 gsm semi-chem packaging paper.

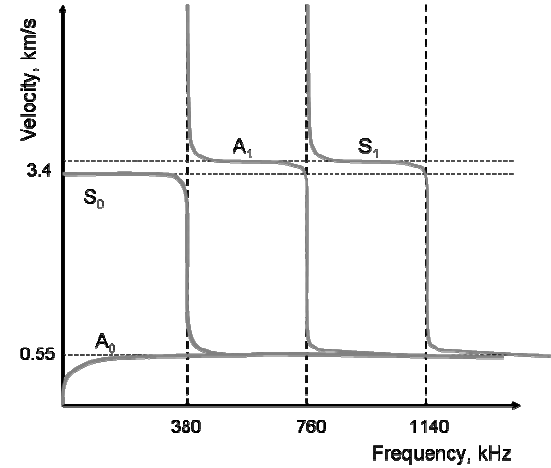


**Figure 10. Theoretical MD dispersion curves generated from elastic constants for SC120 gsm medium. (A0, A1 relate to asymmetric wave modes, S0, S1 are symmetric).**

The TDS method, coupled with suitable wide band response sensors, enables convenient measurement of the dispersion curve patterns for paper by allowing the frequency velocity response of paper samples to be mapped. The ability to undertake such mappings comes from the ability of the TDS type system to separate wave components by their propagation delay and presenting them as discrete frequency components in the frequency domain.

## Summary

A new approach to measuring the elastic properties of paper has been developed. Papers have been characterised and these results compared favourably with measured elastic constants in the literature. The TDS method has been shown to overcome a number of difficulties in traditional sonic measurements of paper. In particular, the issue of alternate propagation paths has not only been resolved, but the additional information becomes a valuable input to the characterisation of the elastic performance of paper.

## References

1. Mann, R.W., Baum, G.A., and Habeger, C.C., Determination of all nine orthotropic elastic constants for machine made paper. IPC Technical Paper Series No. 84, April 1979.
2. Mann, R.W., Baum, G.A., and Habeger, C.C., Elastic Wave Propagation in Paper. Tappi J. August 1979. Vol 68, No. 8.
3. Baum G.A., and Bornhoeft, L.R., Estimating Poisson ratios in Paper Using Ultrasonic Techniques. IPC Technical Paper Series, Number 69. December 1978.
4. Baum G.A., The elastic properties of paper: a review. IPC Technical Paper Series, No. 145. August, 1984.
5. Habeger, C.C., and Whitsitt, W.J., A mathematical model of compressive strength in paperboard. Fibre Science and Technology 19(1983) pp. 215-329
6. Markstrom, H., Testing methods and instruments for corrugated boards. Lorentz and Wettre, 1999.
7. Luukkala, M., and Marttinen, T. Method and apparatus for non-contacting tension measurement in a flat foil and especially in a paper web. U.S. Pat. No. 4, 833, 928.
8. Habeger, C.C., Mann, R.W., and Baum, G.A. Ultrasonics 17:57 (1979)
9. Brodeur, P.H., Hall, M.S., Lorenz, K.W., and Jackson, T.G., Thickness direction measurements in paper materials using ultrasonic sensors immersed in water-filled wheels. IPST technical paper series No. 185. July 1991.
10. Lu, M.T., On-line measurement of strength characteristics of a moving sheet. Tappi J., June 1975, 58 (6).
11. P. H. Brodeur, M. A. Johnson, Y. H. Berthelot, J. P. Gerhardstein. Noncontact laser generation and detection of Lamb waves in paper. Journal of Pulp and Paper Science, 23, J238, (1997).
12. Hall, M.S., Jackson, T.G., and Brown, E., On machine Ultrasonic Sensors for Paper Stiffness - Final Report for the US DOE. April 2000.
13. Van Zummeren, M., Young, D., Habeger C.C., Baum, G. A., and Treleven, R. Automatic determination of ultrasonic velocities in planar materials. IPC Technical Paper Series No. 181, June 1981
14. Habeger C.C., and Baum G.A., On-line measurement of paper mechanical properties. IPC Technical Paper Series No. 157, August 1985.
15. Baum G.A., and Habeger C.C., On-line estimates of strength. IPC Technical Paper Series No. 187, June 1986.

16. Ridgway P., Russo R., Lafond E., Jackson T., Zhang X. A sensor for laser ultrasonic measurement of elastic properties during manufacture.
17. Baum G. A., Polar diagrams of elastic stiffness: effect of machine variables. IPC Technical paper series No. 242. June, 1987.
18. Biering, H., and Pedersen, O., Bruel and Kjaer. Technical Review. System Analysis and Time Delay Spectrometry (Part II). No.2, 1983.
19. Habeger, C.C., Wink, W.A., and Van Zummeren, M.L., Using neoprene-faced, PVDF transducers to couple ultrasound into solids. J Acoustic Soc. Am., October 1988, 84 (4).
20. Vahey, D.W., Correlating the on-line measurement of ultrasonic velocity with strength properties. Tappi J., April 1988, pp 149-152.
21. Vahey, D.W, An ultrasonic based strength sensor for on-line measurements. Tappi J., March 1987. pp. 79-82.
22. Baum G.A., Brennan, D.C., and Habeger, C.C., Orthotropic elastic constants of paper. Tappi J., August 1981, 64 (8).
23. Habeger, C.C., Wink, W.A., Ultrasonic velocity measurements in the thickness direction of paper. Journal of Applied Polymer Science, Vol 32, 4503-4540 (1986).
24. Rose, F., Elastic Waves – On a paper plate. Report from MISG workshop, Newcastle, 1994.
25. Lantz, K.G., and Chase, L.M., On-line measurement and control of strength properties. Tappi J. Feb. 1988. pp 75-78.
26. Baum, G.A., On the verge of total control of the paper-machine. PTI November 1988, pp. 383-390.